



UvA-DARE (Digital Academic Repository)

Preserving the Surface Activity of Lung Surfactant Using Soft Nebulization

Xie, Kaili; Varkevisser, Thijs; Deblais, Antoine; Onland, Wes; van Kaam, Anton H.; Bonn, Daniel; van Rijn, Cees J.M.

DOI

[10.1002/smsc.202400639](https://doi.org/10.1002/smsc.202400639)

Publication date

2025

Document Version

Final published version

Published in

Small Science

License

CC BY

[Link to publication](#)

Citation for published version (APA):

Xie, K., Varkevisser, T., Deblais, A., Onland, W., van Kaam, A. H., Bonn, D., & van Rijn, C. J. M. (2025). Preserving the Surface Activity of Lung Surfactant Using Soft Nebulization. *Small Science*, 5(7), Article 2400639. <https://doi.org/10.1002/smsc.202400639>

General rights

It is not permitted to download or to forward/distribute the text or part of it without the consent of the author(s) and/or copyright holder(s), other than for strictly personal, individual use, unless the work is under an open content license (like Creative Commons).

Disclaimer/Complaints regulations

If you believe that digital publication of certain material infringes any of your rights or (privacy) interests, please let the Library know, stating your reasons. In case of a legitimate complaint, the Library will make the material inaccessible and/or remove it from the website. Please Ask the Library: <https://uba.uva.nl/en/contact>, or a letter to: Library of the University of Amsterdam, Secretariat, P.O. Box 19185, 1000 GD Amsterdam, The Netherlands. You will be contacted as soon as possible.

Preserving the Surface Activity of Lung Surfactant Using Soft Nebulization

Kaili Xie,* Thijs Varkevisser, Antoine Deblais, Wes Onland, Anton H. van Kaam, Daniel Bonn, and Cees J. M. van Rijn*

Inhalable aerosols produced by nebulization offer a promising noninvasive route for lung drug delivery. Yet, high shear stresses during nebulization are highly detrimental to many complex biopharmaceuticals, such as lung surfactants, leading to degradation and further reducing their efficacy. Herein, to mitigate this issue, a novel soft nebulization approach with low-energy input is proposed. Results demonstrate that the lung surfactant aerosolized by soft nebulization undergoes minimal structural alteration and retains its good surface activity in maintaining low surface tension, compared to vibrating mesh nebulization. Upon deposition at the air–liquid interface, the initial spreading of lung surfactant is driven by the Marangoni effect, followed by adsorption and reorganization of lamellar layers. Notably, the lung surfactant using soft nebulization promotes rapid spreading, similar to non-nebulized surfactant, and remains robust under periodic compression–expansion cycles of the interface. The *in vitro* studies present a promising nebulization strategy for preserving both the surface activity and lamellar vesicle structures of surfactant-based drugs, which could be key to enhancing their therapeutic effectiveness in aerosol drug delivery.

air–liquid interface of the alveoli in the lungs. Its critical role is to facilitate breathing and prevent alveolar collapse by maintaining a low surface tension of the interface.^[1–3] The lack of effective lung surfactant, particularly in premature infants (before 37 weeks of gestation), could lead to a pulmonary disease called respiratory distress syndrome (RDS), a potentially fatal disorder characterized by reduced lung compliance and functional residual capacity, causing impaired gas exchange.^[4] Worldwide, about 1% of all newborns develop RDS,^[5] and it has become the leading cause of death in premature infants (50–70% of death in low-income countries).^[6,7] The cornerstone of RDS treatment is the instillation of exogenous surfactant to the lungs, with European data from 2014 to 2016 showing that ≈50% of all infants born between 22 and 32 weeks of gestation require surfactant administration.^[8]

Surfactant replacement therapy (SRT) has been shown to significantly reduce RDS mortality.^[9,10]

The technique development for SRT has been studied for decades. Traditionally, exogenous surfactant was instilled as a bolus through an endotracheal tube inserted into the patient's trachea.^[10,11] Although this approach provides a rapid route for delivering the surfactant to lungs, it is an invasive procedure that may cause significant patient discomfort. Clinicians have adopted a less invasive approach, using a thin catheter placed between the vocal cords to slowly inject the surfactant into the trachea while the baby breathes spontaneously. However, this procedure still requires laryngoscopy, which may also be uncomfortable for the patient. Delivering surfactant via inhalable particles, such as liquid aerosols^[12–15] and dry powders,^[6,16] is considered a truly noninvasive route for surfactant administration. While dry powders are generally considered more stable in formulation and suitable for long-term storage, their production often requires complex and costly processes such as spray drying or spray freeze drying from the liquid formulations. In contrast, surfactant liquid aerosols can be directly generated using nebulization devices, which convert liquid medications into tiny droplets that can be inhaled directly into the lungs.^[17,18] However, a primary barrier to aerosol drug delivery is the large and broad aerosol droplet size distribution produced from nebulization, which hinders drug deposition in deep respiratory regions such as the alveoli. Previously, extensive efforts have


1. Introduction

Lung surfactant is a mixture of lipids and proteins secreted by type II alveolar cells that regulates surface tension at the

K. Xie, T. Varkevisser, A. Deblais, D. Bonn, C. J. M. van Rijn
van der Waals-Zeeman Institute
Institute of Physics
University of Amsterdam
Amsterdam 1098XH, The Netherlands
E-mail: k.xie2@uva.nl; c.j.m.vanrijn@uva.nl

W. Onland, A. H. van Kaam
Emma Children's Hospital
Department of Neonatology
Amsterdam University Medical Center
Amsterdam 1105AZ, The Netherlands

W. Onland, A. H. van Kaam
Amsterdam Reproduction & Development
Amsterdam University Medical Center
Amsterdam 1105AZ, The Netherlands

 The ORCID identification number(s) for the author(s) of this article can be found under <https://doi.org/10.1002/smsc.202400639>.

© 2025 The Author(s). Small Science published by Wiley-VCH GmbH. This is an open access article under the terms of the Creative Commons Attribution License, which permits use, distribution and reproduction in any medium, provided the original work is properly cited.

DOI: 10.1002/smsc.202400639

focused on the fine control of aerosol droplet size in nebulization.^[19] For instance, compared to jet nebulization^[20] and ultrasound nebulization,^[21] more advanced vibrating mesh (VM) nebulization^[22,23] produces a larger fine particle fraction of aerosols and achieves higher levels of lung deposition.^[24]

Nevertheless, in most studies on surfactant aerosolization, little attention has been paid to the preservation of the structure and functionality of the surfactant after nebulization, which are also key factors in determining the delivery effectiveness. In principle, sufficient shear stresses must be applied to break the liquid jets or films into droplets in all nebulization methods. However, the high shear stresses can be detrimental to many biopharmaceuticals with complex structures,^[25] such as lung surfactants. These forces may cause partial to significant drug degradation due to physicochemical and conformational changes. Previous reports^[26] have indicated that protein-based drugs may lose over 70% of their functional activity after 10 min of nebulization using jet and ultrasonic nebulizers. Similarly, denaturation also has been reported in lipid-based particles^[9,27,28] when using VM nebulizers. The particle structures are physically unstable during nebulization, as the shearing and ultrasonic waves can disrupt the lipid membrane layers and fragment the particles, leading to significant deficiencies in the drug particle function.

In current clinical practice, animal-derived surfactants are among the most widely used for surfactant administration, though synthetic alternatives are showing promise.^[29] In both types, evidences^[3,13,30] demonstrate that interactions between lipids and proteins favor the formation of lamellar bodies with an onion-like appearance,^[3,31] which are essential for rapidly creating a lipid film at the air–liquid interface in alveoli to reduce surface tension. An aspect of paramount importance, therefore, is the preservation of this delicate structure. However, little is known about the integrity of the lamellar configuration and its functional activity after nebulization. Ideally, modification of the surfactant during nebulization should be minimal.^[29] Nebulized lung surfactant should also exhibit rapid adsorption and film formation at the alveolar air–liquid interface, while maintaining its surface-active properties throughout the periodic changes in interface area, comparable to untreated surfactant.

In this work, we focus on the dynamic properties and structures of the animal-derived biopharmaceutical lung surfactant at the air–liquid interface before and after nebulization. The lung surfactant is nebulized using a conventional VM nebulizer and a novel soft nozzle (SN) spray, then deposited onto an air–liquid interface in a Langmuir trough, where the spreading dynamics and responses to periodic area changes are investigated. Compared to the VM nebulization, the SN nebulization approach demonstrates better preservation of the lamellar structure integrity in lung surfactant, resulting in the dynamic responses comparable to those of non-nebulized surfactant at the interface. We further elucidate the mechanisms of spreading dynamics, as well as the reversible and irreversible adsorption of the surfactant at the interface. These fundamental understandings offer a promising route for enhancing drug efficacy after nebulization by preserving the structural integrity of the drug.

2. Results and Discussion

2.1. Nebulization and Measurement of Dynamic Surface Properties

Animal-derived lung surfactant from poractant alfa (Chiesi, Parma, Italy) was nebulized using a recently advanced VM nebulization and a novel SN spray to produce aerosols (Figure 1a,b, and Video S1, S2, Supporting Information), see details in Experimental Section. The reason for choosing these nebulization approaches is that jet and ultrasound nebulization have been shown to be generally unsuitable for sensitive biopharmaceuticals due to inherent limitations, such as exposing drugs to repeated shear stresses from the recirculation of large aerosol droplets.^[23,26,32] Initially, the surfactant has an aqueous formulation containing particles composed of a mixture of phospholipids and proteins (Figure S1, Supporting Information), which is distinct from phospholipids that are first dissolved in organic solvents such as chloroform. The principle of generating aerosols in these two nebulization methods is similar, both utilizing Rayleigh breakup of extruded liquid jets as they pass through either the mesh or the nozzles (images in Figure 1a,b); however, the difference is that our SN spray is passive, relying solely on mechanical squeezing of the surfactant solution through the nozzles, while VM nebulization is active, involving ultrasound waves from the high-frequency vibration of the mesh.^[33]

To characterize the dynamic surface properties, that is, dynamic surface tension, of the lung surfactant before and after nebulization, we deposited the non-nebulized and nebulized surfactant solutions onto an air–liquid interface formed in a Langmuir trough^[34] at a controlled temperature of 37 °C (Figure 1c). To quantify the amount of nebulized surfactant deposited, rather directly depositing the surfactant aerosols onto the interface, we first collected the aerosols in a centrifuge tube (15 mL) and then applied the liquefied aerosol solution onto the interface using a precise syringe pump (see Experimental Section). The surface tension was measured spontaneously using a platinum Wilhelmy plate. Periodic changes of the interface area can be achieved by the oscillatory motion of a leakage-free barrier in the trough (Figure S2, Supporting Information).

Figure 1d shows that once the lung surfactant reaches the air–liquid interface, the surface tension, γ , first rapidly decreases (within a few seconds) and eventually reaches a plateau at $\approx 25 \text{ mN m}^{-1}$. A lower surface tension cannot be achieved by adding more surfactant (Figure S3, Supporting Information), indicating that the surfactant molecules fully cover the interface. This surface tension at equilibrium is consistent with previous reports on lung surfactant.^[13,35,36] Since the most functional phospholipid in lung surfactant for reducing surface tension is dipalmitoylphosphatidylcholine (DPPC),^[31] we also introduced DPPC in chloroform formulation and DPPC vesicle dispersion in aqueous formulation onto the air–liquid interface as control experiments (see Figure S4, Supporting Information). Figure 1d shows that, compared to lung surfactant, DPPC in the chloroform formulation spreads more rapidly at the interface to reduce surface tension but reaches the same final value as the lung surfactant. In contrast, the deposition of an aqueous dispersion of DPPC vesicles does not reduce the surface tension. This is as the DPPC vesicles remain intact at the interface, showing no surface

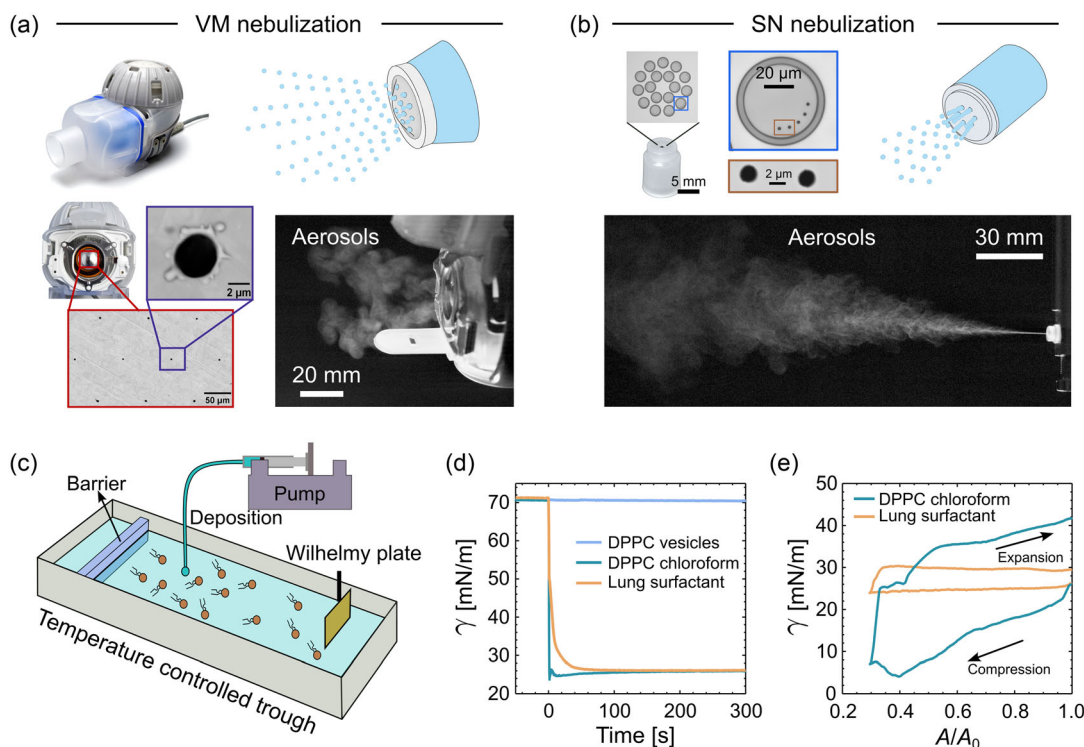


Figure 1. Experiments. a) VM nebulizer (Pari eFlow rapid) and its pore size on the mesh. The aerosols are produced by squeezing the liquid through the mesh by the high-frequency vibration of the mesh. b) SN spray (Medspray) and its nozzle size. The aerosols are produced by mechanically pushing the liquid through the nozzles. c) Langmuir trough. The surfactant is deposited using a syringe at the air–liquid interface, and the spontaneous surface tension is measured using a Wilhelmy plate method. The temperature of trough is fixed at 37 °C. d) Surface tension as a function of time for different preparations of surfactant/lipids. e) Surface tension variation with surface area. The surface area changes at a rate of 13.5 cm² min⁻¹, a slow mode. The concentrations of lung surfactant and DPPC lipid in (d,e) are same (10 mg mL⁻¹) for all preparations, see experimental details in Supporting Information. The close-up images of VM and SN were captured using a scanning electronic microscope.

flow induced (Figure S4b, Supporting Information). It requires a high-energy input to disrupt the lipid bilayer of the vesicles and release sufficient surface-active lipid molecules at the interface to reduce surface tension.^[37,38]

Figure 1e depicts the surface tension dynamics during the compression–expansion cycle of the interface area. Here, the compression begins from an initial area A_0 and reaches 30% of A_0 , followed by expansion. The lung surfactant demonstrates an excellent ability to maintain a relatively constant surface tension throughout the cycle. However, DPPC in the chloroform formulation shows lower surface tension (reaching the collapse point)^[39] under compression, but the surface tension becomes twice as high when the surface area recovers to its initial value. Therefore, using either DPPC vesicles or DPPC solvent-spread films alone to study the surface dynamic properties may oversimplify the behavior of lung surfactant interfacial structures as they may exist in vivo and is not applicable for SRT.^[40]

2.2. Spreading Dynamics at the Air–Liquid Interface

We here investigate the spreading dynamics of lung surfactant prepared with different nebulization methods by depositing the surfactant onto the initially clean air–liquid interface in the Langmuir trough. **Figure 2a** illustrates that the surfactant nebulized by the SN method completes spreading in ≈ 20 s,

which is similar to the timescale for the non-nebulized surfactant. In contrast, it takes significantly longer (≈ 120 s) for the surfactant nebulized by the VM method to reach equilibrium. These results plausibly indicate that the VM method deactivates part of the lung surfactant, leading to a slower response in reducing surface tension during spreading dynamics. At equilibrium, all surfactants yield the same steady surface tension (≈ 25 mN m⁻¹). This is because the surfaces are fully covered by the surfactants (Figure S3, Supporting Information). A question thus remains: What does the VM nebulization change in the lung surfactant?

To understand this, we first applied light scattering to measure the particle size distribution of lung surfactants processed using different methods (see Experimental Section). As shown in Figure 2b, the non-nebulized lung surfactant and the one nebulized by SN method each show only one peak in the size distribution, giving particle mean diameters 6.5 and 3.6 μm, respectively. However, two peaks appear using VM nebulization, located around 170 nm and 3.3 μm, with the smaller size peak dominating. Although both nebulization methods reduce the surfactant particle size, the VM method apparently produces more nanoscale particles that are one order of magnitude smaller than those produced by the SN method. Small surfactant particles at the nanoscale appear to be responsible for slowing down the spreading dynamics. To verify our observation, we further deposited surfactant with a size distribution similar to that of

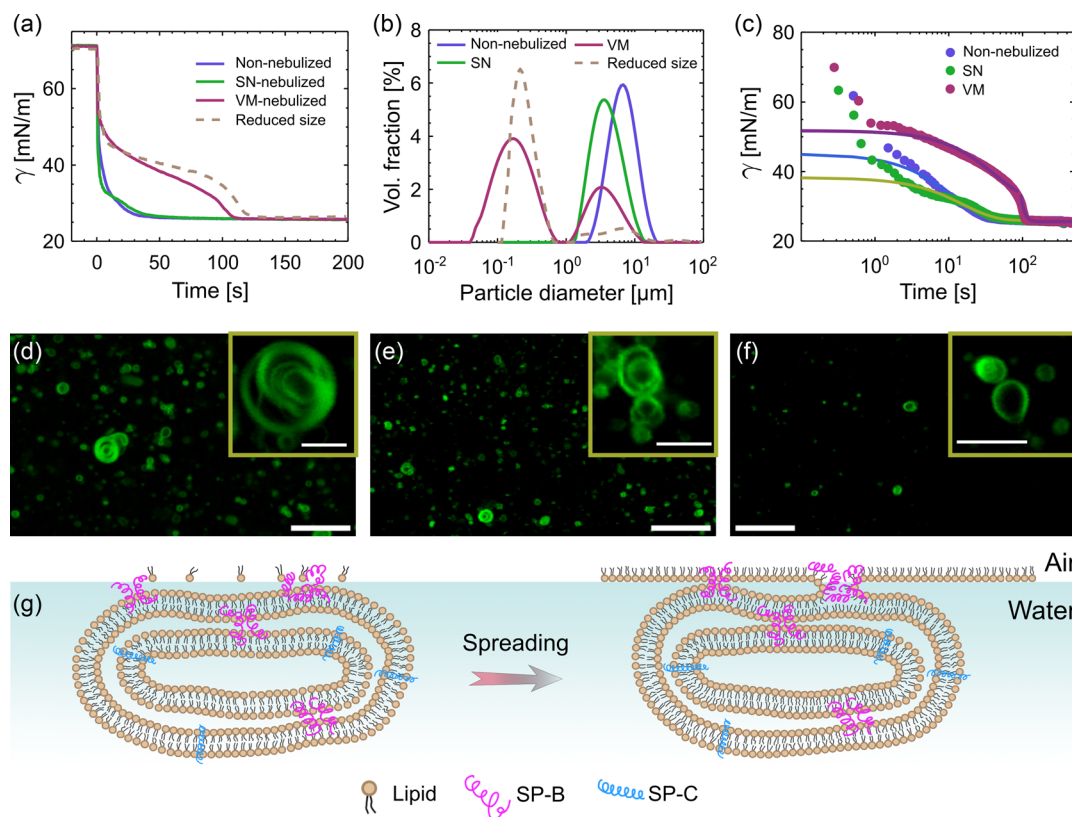


Figure 2. Dynamic surface tension in spreading and lung surfactant structures. a) Surface tension variation with time upon deposition of the lung surfactant with different preparations. Here, 20 μL of surfactant with a concentration of 10 mg mL^{-1} was applied onto an initially clean liquid surface in all experiments. The reduced size surfactant is prepared by passing the raw surfactant through a 200 nm filter. b) Lung surfactant particle size distribution measurement using light scattering. c) Relaxation model fit with the data in (a) plotted on a semilogarithmic scale. d–f) Confocal microscope images of lung surfactant: non-nebulized surfactant (d), nebulized by SN (e), and VM (f). Scale bars are 20 μm in the main panels and 5 μm in the insets. Lamellar body-like structures are observed in the non-nebulized and SN-nebulized surfactants, while VM disrupts the layers and significantly degrades the structures. g) Schematic representation of the adsorption and spreading of lung surfactant with lamellar structures at the air–liquid interface.

the VM, but prepared by being squeezed through a 200-nm pore-size membrane driven by mechanical pressure (dashed line in Figure 2b). This surfactant with reduced particle size exhibits a similar spreading behavior as that of the VM nebulization (dashed line in Figure 2a).

The kinetics of surfactant spreading at the air–liquid interface is not driven by diffusion, as the reduction in surface tension ($\gamma_0 - \gamma$) does not follow the diffusive scaling of $\approx t^{1/2}$ (see Figure S5, Supporting Information). Figure 2c, showing the same raw data as in Figure 2a but on a semilogarithmic scale, highlights that the dynamic surface tension follows well the exponential equation

$$\gamma = \gamma_{\text{eq}} + \beta e^{-t/\tau} \quad (1)$$

where γ_{eq} is the surface tension at equilibrium and β and τ are the prefactor and relaxation time, respectively. This model has already been used to describe the kinetically limited adsorption of ionic surfactants^[41] and polymers^[42] at the interface. It accounts for the process that is hindered by adsorption barriers. However, this model cannot account for the dynamics of all surfactants in the very early stage ($t < 3$ s) in our experiments. The reason for this

will be discussed later. Here, the relaxation time indicates the rate at which the surfactant organizes and adsorbs at the interface before reaching equilibrium. Therefore, it provides an estimate of the mobility of the surfactant molecules at the interface. **Table 1** shows the relaxation times for different preparations of lung surfactants, calculated using Equation (1). SN nebulization gives similar relaxation time to the non-nebulized surfactant. However, the kinetic behavior of VM-nebulized surfactant cannot be described by a single-exponential fit but requires a double-exponential model to account for the two characteristic relaxation time scales, yielding 42.5 s for the first stage and 11.2 s for the second stage (Figure 2c). This indicates that there may be two processes involved in the organization of VM-nebulized surfactant at the interface. The large relaxation time explains the slow dynamic response in surface tension reduction.

Table 1. Relaxation time of lung surfactant in spreading kinetics.

	Non-nebulized	SN-nebulized	VM-nebulized
τ [s]	11	13.7	42.5 11.2

We further examined the particle structures of lung surfactant under different preparations using a confocal laser scanning microscope (CLSM); see details in Experimental Section. As shown in Figure 2d, most of the non-nebulized surfactant particles exhibit typical ultrastructural features, primarily consisting of a lamellar body-like structure. This typical structure has also been confirmed by previous works^[13,43] using transmission electron microscopy. SN nebulization can generally preserve the lamellar body-like structure of the surfactant (Figure 2e), but it may reduce the number of lamellar layers since the particle size is slightly decreased. However, VM nebulization significantly degrades the surfactant particle structure, resulting in a single-layer predominated structure in most particles (Figure 2f). Moreover, the particles are much less visible under CLSM, which further confirms that most particles after VM nebulization are at the nanoscale (Figure 2b). These rudimentary structures and nanoscale particles resulting from VM nebulization are thus the main factors that lead to slow spreading dynamics. There is less surface-active surfactant remaining after using the VM nebulization method. The amount of surfactant deactivated by the VM method can be estimated using the surface pressure-area isotherm^[44,45] (see Figure S6a, Supporting Information), where the surface pressure is defined as the difference in surface tension between the surfactant-covered surface and the clean surface. As the surface area decreases, the surfactant concentration at the interface increases, leading to a rise in surface pressure, eventually reaching a plateau of $\approx 45 \text{ mN m}^{-1}$ (Figure S6, Supporting Information). It is found that the VM nebulization method can result in a loss of $\approx 15\text{--}20\%$ of active surfactant compared to the non-nebulized one. The loss of surfactant activity primarily arises from the shear stresses in aerosolization process itself—breaking the liquid into droplets—rather than subsequent coalescence, even though significant droplet coalescence occurs in the aerosol mist (see Videos, Supporting Information).

Extensive previous works^[3,46,47] have illustrated that the lamellar body, with its onion-like structures, is the result of the interaction between phospholipids and proteins, which play a crucial role in lung mechanics. The proteins, such as hydrophobic SP-B and SP-C, are membrane associated. Surfactant protein SP-B bridges both the bilayers and monolayers of lipids through interfacial interactions, while SP-C preferentially inserts into the phospholipid membrane with a transmembrane orientation (see schematic in Figure 2g). The lamellar structure facilitates the unfolding of lipid layers and their adsorption to the air–liquid interface at a low-energy cost in the presence of the proteins. Once the surfactant particles reach the interface, the proteins create hydrophobic cavities that stabilize lipid molecules at the interface through a structural change of the lamellar bodies,^[30] leading to a rapid reduction in interfacial tension. In addition, the proteins could also act as nucleation defects^[48] in the lipid membrane, facilitating pore formation to destabilize the lipid bilayer structures at a reduced energy consumption. The energy^[49] to create a pore of radius r_p is estimated as $E = 2\pi r_p \sigma - \pi r_p^2 \gamma_s$, where σ is the line tension at the pore edge and γ_s is the tension in membrane. The activation energy for a pore formation is thus given by $\Delta E = \pi \sigma^2 / \gamma_s$. Considering the pure DPPC bilayer vesicles (without defects) with a surface tension $\gamma_s \approx 10^{-3} \text{ N m}^{-1}$ and line tension $\sigma \approx 10^{-10} \text{ N}$, we can obtain an energy of $\approx 10^3 k_B T$ to disrupt the lipid layer, where k_B is the

Boltzmann constant and T is temperature, which is remarkably large. This estimation also supports our observation that the DPPC vesicles in aqueous dispersion are not effective in reducing surface tension (Figure 1d), as most vesicles remain intact at the air–liquid interface.

Nebulization, such as the VM method shown in this work, destroys the lamellar structure of the surfactant particles by depleting proteins from the lipid layers. This destruction appears difficult to repair, for example, through self-assembly driven by thermodynamics and interactions among lipid and protein molecules, at least within the time scale of our experiments. This is confirmed by our measurements of surfactant particle size distribution over time. As shown in Figure S7, Supporting Information, after 4 h, there is almost no change in the particle size distribution of surfactant nebulized using the VM method. A lower amount of proteins in the phospholipid membrane renders the particles (vesicles) more stable. This limits the transfer of lipid molecules from the membrane to the air–liquid interface, resulting in a slower response to surface tension reduction and a longer relaxation time. Preserving the phospholipid–protein structural integrity of lung surfactant is therefore crucial for rapid adsorption to the air–liquid interface.

As mentioned above, in Figure 2c, the relaxation model fails to describe the dynamic behavior in the early stage ($t < 3 \text{ s}$) for all surfactant preparations. The surface tension drops from 70 mN m^{-1} to roughly 50 mN m^{-1} within $\approx 2 \text{ s}$, much faster than what is expected for surfactant reorganization and adsorption at the air–liquid interface. Moreover, this faster reduction in surface tension seems to be independent of whether the surfactant is nebulized (early stage in Figure 2c). To understand the mechanism behind, we applied particle image velocimetry (PIV) to get insights into the surface flow dynamics after surfactant drop deposition (see details in Experimental Section). After surfactant deposition at the air–liquid interface, a rapid nonuniform distribution of surfactant concentration over the surface is created. The surface thus flows driven by the Marangoni effect.^[50] A surface tension gradient, $\partial\gamma/\partial l$, where l is the characteristic length, is formed, driving the surface flow at velocity u . This capillary force is balanced by the viscous drag force, $\partial\gamma/\partial l = \eta \partial u / \partial h$, where η is the viscosity and h is the depth of surfactant layer near the interface. This leads to a characteristic surface velocity.

$$u^* = \frac{h \Delta\gamma}{\eta \Delta l} \quad (2)$$

Figure 3 shows the typical results of our PIV measurements. Upon surfactant drop deposition, surface flow moves the tracer particles outward from the center of the Petri dish (see Video S3, Supporting Information). The velocity u in Figure 3c represents the radial peak velocity, averaged along the circumference of the ring (the boundary of the clean area) in Figure 3b. No significant difference in the average velocity was observed for the different lung surfactant preparations. The flow begins to slow down at 0.2 s after the surfactant deposition. This is primarily due to the edge of the clean area approaching the boundary of the Petri dish (Figure 3a). We thus take the Marangoni flow velocity $u \approx 45 \text{ mm s}^{-1}$ and compute the timescale of surfactant spreading in the Langmuir trough, yielding a characteristic time $t = \Delta l / u \approx 2.2 \text{ s}$, where the surfactant was deposited 10 cm (Δl) away

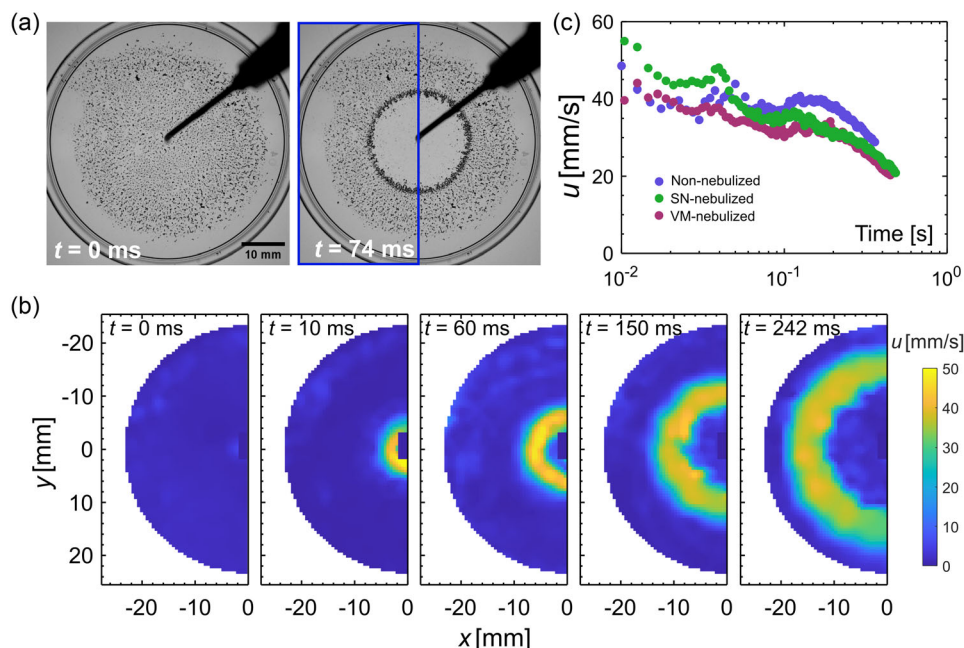


Figure 3. Surface flow upon surfactant deposition. a) Optical images of surfactant drop deposition on the saline water surface using a Teflon needle. The water surface is initially covered by hollow silver-coated glass particles. Once the surfactant drop is deposited, the flow drives the particles to move outward, forming a clean area in the center. Blue rectangle represents the region of interest in velocity field shown in (b). b) Time-lapsed velocity field calculated from PIV. Only half of the velocity field is represented. The velocity in the center area (within the ring) is actually not zero. The velocity field here shows “zero” just because of no particles detected in PIV calculation. c) Radial peak velocity averaged along the circumference of the clean area front. The concentration of lung surfactant is 10 mg mL^{-1} , and the deposition volume is $2 \mu\text{L}$ in all experiments.

from the Wilhelmy plate. This timescale is in good agreement with the observed rapid reduction in surface tension shown in Figure 2a,c and explains the discrepancy with the relaxation model in Equation (1). Marangoni flow dominates the spreading dynamics in the early stage of surfactant spreading. Taking $u \approx 45 \text{ mm s}^{-1}$, $\eta = 10^{-3} \text{ Pa s}$, $\Delta l = 10 \text{ cm}$, and $\Delta\gamma \approx 22 \text{ mN m}^{-1}$ into Equation (2), we can simply estimate the transport depth of the surfactant into the subphase, yielding $h \approx 225 \mu\text{m}$. This value is consistent with the dark-field microscopy measurement,^[37] where very few lipid particles are observed at the focal plane $420 \mu\text{m}$ below the air-liquid interface.

2.3. Dynamic Surface Activity in Response to the Area Change

Here, we assess the surfactant activity from different preparations under the harmonic oscillations of the air-liquid surface area. Once the surfactant has fully spread at the interface, a waiting duration of $\approx 5\text{--}10 \text{ min}$ is applied to allow the surfactant to relax. We always begin with the compression from the initial maximum surface area, followed by expansion. Figure 4 shows the dynamic surface tension of the lung surfactants prepared with and without nebulization. The surface area change is set to a slow mode ($13.5 \text{ cm}^2 \text{ min}^{-1}$) with a maximum area change of 40% of the initial area. The surfactant nebulized using the SN method shows a similar response to area changes as the non-nebulized surfactant, with surface tension oscillating around 27 mN m^{-1} . This trend is maintained until the sixth cycle (Figure 4a), indicating that the surfactant activity at the interface during the compression-expansion process is reversible.

However, the surface tension of VM-nebulized surfactant begins to deviate from that of the non-nebulized surfactant from the second area expansion, showing a reduced ability to maintain the surface tension. After nine cycles of compression-expansion, the surface tension shows no remarkable difference among the surfactants with the different preparations. The reason for this is the dissociation of surfactant from the interface during compression, as discussed later.

One critical criterion for assessing the performance of lung surfactant is that the surfactant is capable of respreading rapidly and reversibly upon area expansion while maintaining low surface tension. Here, we investigate the minimum surface tension, γ_{\min} (occurring in compression), and maximum surface tension, γ_{\max} (occurring in expansion), during the area compression-expansion cycles. As shown in Figure 4b,c, γ_{\min} is around 25 mN m^{-1} and shows a weak dependence on the number of cycles and the surfactant preparations. However, γ_{\max} shifts from ≈ 30 to $\approx 40 \text{ mN m}^{-1}$ during expansions for the VM-nebulized surfactant, indicating the occurrence of irreversibility in the surfactant activity at the interface. This is also, in general, consistent with our earlier observation that there are more ineffective surfactant particles after using VM nebulization. In Figure 4, the duration of area expansion in the experiments is 160 s . This timescale is much longer than the time required for the non-nebulized and SN-nebulized surfactants to reach equilibrium ($\approx 20 \text{ s}$), but is similar to the timescale for the VM-nebulized surfactant to reach equilibrium ($\approx 120 \text{ s}$). The long area expansion time allows the non-nebulized and SN-nebulized surfactants sufficient time to reorganize and establish readsorption at the

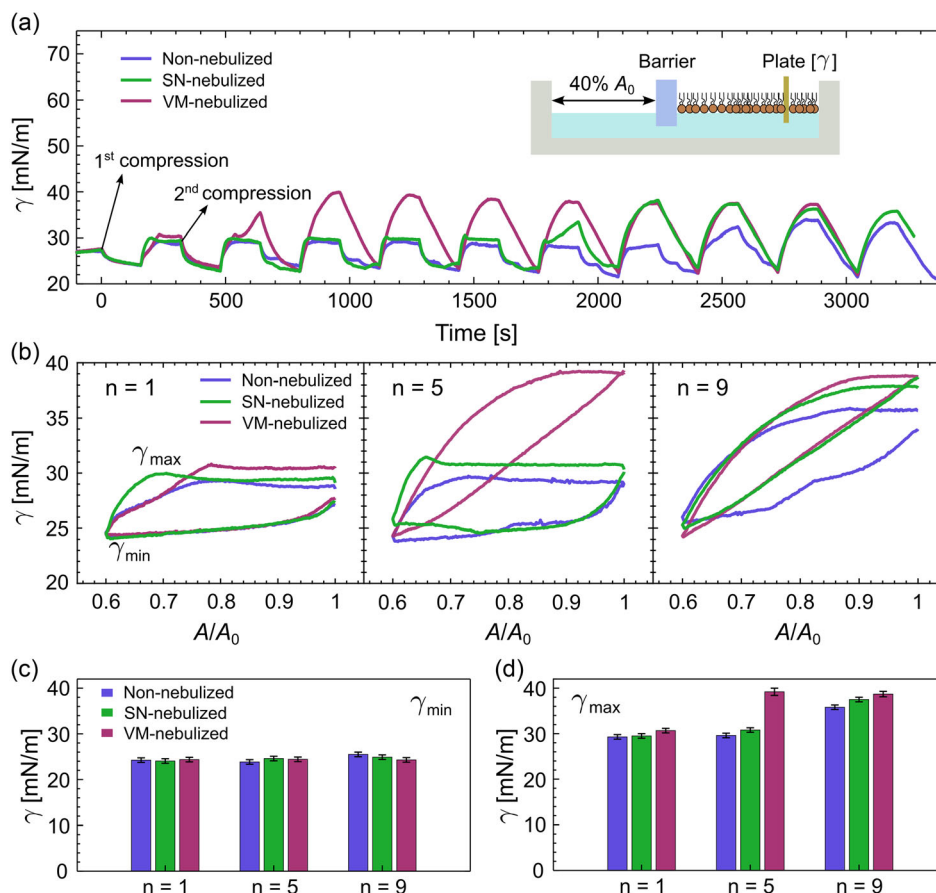


Figure 4. Dynamic surface tension of lung surfactant with different preparations under periodic change of surface area. a) Surface tension versus time during periodic area change in Langmuir trough. The maximum compressed area is 40% of the initial area (inset). The first compression is performed after the films reach the equilibrium. b) Surface tension variation with relative surface area after different numbers of cycles ($n = 1, 5$ and 9). c, d) Minimum (γ_{\min}) and maximum (γ_{\max}) surface tension after different numbers of cycles. Here, the surface area change rate is $13.5 \text{ cm}^2 \text{ min}^{-1}$, a slow mode.

air–liquid interface, as indicated by the appearance of plateaus in surface tension upon expansion. Indeed, upon expansion, the surface tension takes around 30 s to rise from the minimum value to reaching the plateau for the non-nebulized and SN-nebulized surfactants. This timescale is consistent with the spreading timescale (20 s) needed to reach the equilibrium, as shown in Figure 2a, further confirming the established adsorption of the surfactants during the area expansion at the interface. However, during the expansion, the VM-nebulized surfactant does not have enough time to respread and fully cover the surface, resulting in a higher maximum surface tension.

We further examine the influence of the amplitude and rate of surface area change on the γ_{\min} and γ_{\max} during the compression–expansion cycles. As shown in Figure 5a–c, the amplitudes of area change (20, 40, and 70% of A_0) have a weak effect on the γ_{\min} for different surfactant preparations. However, the γ_{\max} does exhibit remarkable differences among the surfactants with various preparations under different amplitudes. At the small amplitude (20% A_0), the oscillations of surface tension are repeatable across different compression–expansion cycles, with stable values for both γ_{\min} (25 mN m^{-1}) and γ_{\max} (30 mN m^{-1}) for all surfactant preparations (Figure 5a). Nevertheless, at the intermediate amplitude (40% A_0), γ_{\max} begins to increase with

the number of cycles and reaches a plateau ($\approx 40 \text{ mN m}^{-1}$), depending on the surfactant preparations (Figure 5b). The γ_{\max} in the VM-nebulized surfactant exhibits less stability in maintaining its value during area expansion compared to the SN-nebulized surfactant.

At the large amplitude (70% A_0) of surface area change (Figure 5c), the increase in γ_{\max} becomes more pronounced and occurs earlier. This demonstrates that the large amplitude of the area change might induce irreversible changes in the surfactant film at the air–liquid interface, leading to poor read-sorption of the surfactant to the interface, even though the duration of the area expansion is longer than the characteristic timescale of surfactant respreading. The irreversible modification of the surfactant is more evident in the VM-nebulized surfactant than in the SN-nebulized one. Indeed, during normal breathing, the lungs undergo a total volume change of $\approx 20\%$, which corresponds to $\approx 10\%$ area change in each compression–expansion cycle.^[51] In such situation, both the VM and SN nebulization methods can effectively produce lung surfactant aerosols that can maintain the surface tension at $\approx 30 \text{ mN m}^{-1}$ (Figure 5a). However, during deep breathing,^[52,53] the surface area of the lungs can increase by more than 40%, during which the SN-nebulized surfactant shows more promise in

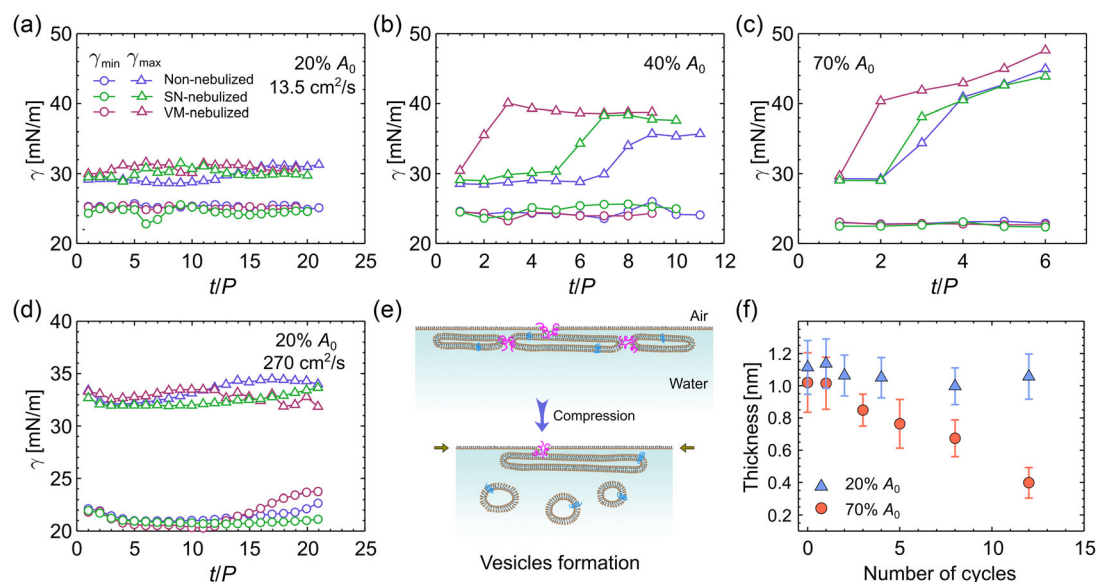


Figure 5. Effects of amplitude and rate of surface area change on the surface tension during periodic cycles. a–d) The maximum and minimum surface tensions during the cycles for different preparations of lung surfactant. The amplitudes are 20, 40, and 70% of A_0 (where A_0 is the initial surface area), with an area change rate of $13.5 \text{ cm}^2 \text{ min}^{-1}$ in (a–c), while the amplitude is 20% A_0 with a $270 \text{ cm}^2 \text{ min}^{-1}$ in the area change rate in (d). The time t is normalized by the period P in each test. P is 160, 320, and 560 s for area changes of 20, 40, and 70% of A_0 , respectively. e) A schematic model illustrating the squeezing-out of lung surfactant reservoirs at the air–liquid interface. The excess surfactant dissociated from the interface is ejected into the bulk, forming closed vesicles. f) The overall film thickness after different numbers of film compression. After each compression, the film area is restored to the initial surface area before measuring the thickness. The error bars indicate the standard deviation from 3–5 different measurements.

maintaining reversible low surface tension compared to the VM method.

In Figure 5a,d, we next compare the influence of the rate of surface area change on γ_{\min} and γ_{\max} for surfactants nebulized using different methods. Two modes are used (slow mode: $13.5 \text{ cm}^2 \text{ min}^{-1}$; fast mode: $270 \text{ cm}^2 \text{ min}^{-1}$). It depicts that the surface tension hovers within a slightly larger range ($20\text{--}35 \text{ mN m}^{-1}$) in the fast mode compared to the range ($25\text{--}30 \text{ mN m}^{-1}$) in the slow mode. γ_{\min} and γ_{\max} remain roughly constant and show a weak dependence on the surfactant preparations in both modes. Note that the amplitude of the area change is 20% A_0 in these two modes. These observations show that both VM and SN nebulization methods can result in reversible respreading and readsorption of the surfactant at the air–liquid interface when the amplitude of the surface area change is small. Furthermore, Figure 5a–d illustrates that the dynamic surface activity of the surfactant at the interface is more sensitive to the amplitude of the area change but is weakly dependent on the rate of the area change. In fact, the respiratory rate in neonates varies considerably, ranging from 0.5 to 1 Hz.^[54] In our experiments, the maximum frequency of the surface area change is about 0.1 Hz, limited by the device. Although this cannot replicate the actual breathing rates of neonates, the results can offer fundamental insights into the dynamic behavior of lung surfactant with various nebulization methods in response to lung area changes in breathing.

2.4. Discussion

The capability of lung surfactant to rapidly and reversibly readsorb onto the air–liquid interface upon expansion after

compression reflects its effectiveness in achieving and maintaining a low surface tension of the air–liquid interface in alveoli. In our experiments, we always begin the first compression with a steady surface tension ($\gamma \approx 25 \text{ mN m}^{-1}$). This surface tension value roughly corresponds to a surface pressure $\pi \approx 45 \text{ mN m}^{-1}$ (see Figure S6, Supporting Information), indicating that the interface has already been fully saturated with the surfactant molecules. In Figure 5, we deposited $20 \mu\text{L}$ of surfactant with a concentration of 30 mg mL^{-1} onto an initial surface area $A_0 = 90 \text{ cm}^2$ in each experiment. If all the surfactant molecules remain at the interface, the molecular area is roughly 0.018 nm^2 per molecule. (The calculation is based on the DPPC molecular weight.) This is much smaller than the molecular area at which the surface pressure plateau appears in the isotherm shown in Figure S6, Supporting Information. How does the surfactant organize at the interface?

Our observations in Figure 2d, along with previous reports,^[3,13,31] demonstrate the multilayer, lamellar body-like structures in lung surfactant. We therefore speculate that, at equilibrium, the adsorbed surfactant film is not simply a monolayer near the air–liquid interface but forms a multilayer with the assistance of membrane-associated proteins (i.e., SP-B and SP-C) due to the excess surfactant molecules (see model in Figure 5e). The multilayer surfactant film beneath the interface is referred to as the surfactant reservoir.^[31,55] Upon compression, the surfactant film undergoes a conformation change: surfactant molecules are squeezed out from the top layer into the surfactant reservoirs. The mechanical stability of these reservoirs varies depending on the amplitude of interface area change as well as the nebulization methods. With a large amplitude (i.e., 70% A_0), the reservoirs

may dissociate from the membrane and be ejected into the bulk to form closed vesicles. This irreversible process leads to a partial loss of the surfactant's active properties at the interface (Figure 5e, bottom). In contrast, under a small amplitude, the surfactant reservoirs remain attached to the interface thanks to the surfactant proteins and serve as a source to respread surfactant onto the interface during the surface area expansion. In Figure 5f), the overall film thickness at the interface after various compression–expansion cycles provides the evidence for both the reversible and irreversible processes.

The classical model for surfactant during compression is based on the selective exclusion of surfactant compounds through the so-called squeeze-out process.^[31,43,56] Unsaturated lipids, such as phosphatidylglycerol (PG) and dioleoylphosphatidylethanolamine (DOPE), struggle to achieve high packing densities during compression due to the presence of double bonds in their chains.^[3] As a consequence, they are more likely to be squeezed out from the interface compared to saturated lipids like DPPC. Therefore, the larger the compression, the greater the fraction of DPPC lipid molecules that remain at the interface.^[57] This supercompressed lipid film is metastable. Once it collapses, surfactant vesicles irreversibly form from the film. Although surfactant proteins can promote the rearrangement and readsorption of these lipid vesicles to the interface, the process of transport from the bulk to the interface takes much longer, primarily due to the limited diffusion of vesicles.^[38] Consequently, this gives rise to an increase in the γ_{\max} upon the area expansion, particularly after several compression–expansion cycles (Figure 5a–c).

The lung surfactant nebulized using the VM method shows a slower dynamic response in spreading and less stability in maintaining surface tension at a low value during interface area expansion, compared to the non-nebulized and SN-nebulized surfactants (see Figure 2, 5). The evidences in this work demonstrate that the significantly degrading surfactant structure resulting from the VM nebulization leads to a diminished ability for efficient film respreading and readsorption at the air–liquid interface during the area expansion. This is mainly attributed to the higher energy input during the VM nebulization method to produce aerosols compared to the SN method ($\approx 35 \text{ J g}^{-1}$ in VM while $\approx 2 \text{ J g}^{-1}$ in SN).^[27,28] The increased energy input negatively impacts the lamellar structures of lung surfactant by disrupting membrane connections and depleting surfactant proteins from the membrane.^[13] Consequently, there are fewer active surfactant reservoirs for the VM-nebulized surfactant film at the interface. Upon expansion, the surfactant transport from these reservoirs to the interface is insufficient to maintain a low surface tension. Our rationalization is based on a microscopic perspective, focusing on structural changes during nebulization. While direct measurements of local energy dissipation-related changes in particle membranes, such as intermolecular forces and protein integrity, would provide greater precision, they are experimentally challenging due to the complexity of lung surfactant.^[3] Molecular dynamic simulations^[58] could potentially address these challenges; however, careful consideration is required to accurately model the molecular interactions between the different components. Alternatively, simplified artificial surfactant compositions, such as DPPC combined with surfactant proteins B and/or C,^[45] could serve as a blueprint to quantify

specific degradations in lipid layers and/or protein integrity during different nebulization methods, such as using the Western blot^[59] or circular dichroism^[60] technique for detecting protein denaturation. Nevertheless, it is worth noting that SP-B and SP-C proteins have molecular weights of 8.7 and 3.7 kDa, respectively, which are relatively small. A recent study^[61] demonstrated that dornase alfa, a much larger protein (29.2 kDa), can maintain its integrity during mesh nebulization. Therefore, protein stability across different nebulization methods remains an open question. Future studies specifically investigating surfactant protein integrity under various nebulization conditions would provide valuable insights.

In the translation of aerosol delivery, there are only a few documented clinical data^[24,62] on deposition efficiency and drug efficacy in preterm neonates. The recommended dose of exogenous lung surfactant for treating RDS is weight dependent on the neonates (see details in Supporting Information). Since the respiratory airways in neonates are much narrower than in adults, fine control of aerosol droplet size distribution is another key factor that may pose a barrier to effective drug delivery. For deposition in the deep respiratory region, the mass median aerodynamic diameter (MMAD) of aerosols is preferred to be 1–5 μm . One limitation of this work is that both VM and SN nebulization produce larger aerosol droplets due to the occurrence of significant droplet coalescence in the aerosol mist.^[63] Previous studies reported that the MMAD of aerosols generated by VM nebulizers ranges from 3.3 to 5.4 μm ,^[64] while SN sprays produce aerosols of ≈ 4.8 –5.7 μm under well-controlled conditions.^[65] Strategies to mitigate aerosol droplet coalescence are therefore needed in future studies to control the surfactant aerosol size. For instance, charging aerosol droplets by applying an electric field during nebulization^[66] is a promising approach to reducing the likelihood of droplet collisions in the mist. Another open question following this work is how other different nebulization methods influence the surfactant structures and surface activity, such as traditional jet and ultrasound nebulizers. Some proteins and lipid-based particles have been shown to degrade using these methods due to repeated shear stresses or temperature increases.^[26–28] However, the extent to which lung surfactant structures are altered after nebulization remains unclear. This study lays the foundation for future systematic investigations using various nebulizers, including evaluating surfactant retention of surface activity, aerosol generation and deposition efficiencies, and suitability for different lung surfactant types, including animal-derived and synthetic formulations. In summary, to achieve enhanced therapeutic effectiveness, both preservation of lung surfactant particle structures and fine control of aerosol droplets are encouraged to be optimized to further advance the SN nebulization approach.

3. Conclusion

In summary, we have investigated the dynamic behaviors of animal-derived lung surfactant at the air–liquid interface using VM nebulization and SN spray methods. We have shown that, upon deposition of the surfactant at the interface, the initial spreading dynamics is dominated by Marangoni flow, followed by the adsorption of complex lamellar layers of the surfactant at

the interface to further reduce surface tension. The latter process is significantly influenced by the nebulization methods. We have further demonstrated that preserving the lamellar structures of lung surfactant using the SN spray method can retain its surface activity, similar to that of the non-nebulized surfactant. This novel method results in the nebulized surfactant rapid spreading at the interface and excellent stability in maintaining low surface tension during periodic area changes. Moreover, we have revealed that surfactant depletion at the interface during periodic area changes is more sensitive to the amplitude of the area change but weakly dependent on the rate of the area change. It is likely that large amplitude induces irreversible changes in the surfactant film at the interface, dissociating surfactant reservoirs from the film and ejecting them into the bulk to form closed vesicles. This irreversible process becomes more pronounced for the surfactant nebulized using the conventional VM method compared to the SN spray method. Our study proposes a low-energy input nebulization method to improve the preservation of lung surfactant's structural integrity when producing aerosols, providing insights for physiological trials aimed at enhancing the efficacy of aerosol drug delivery to the lungs.

4. Experimental Section

Materials and Sample Preparations: Animal-derived surfactant (poractant alfa, 80 mg mL⁻¹ of phospholipids from Chiesi Pharmaceutical, Parma Italy) was kindly provided by Chiesi Pharmaceuticals BV. This surfactant was approved for clinical use. The surfactant, initially in an aqueous formulation, was diluted in experiments using a buffer solution consisting of 0.1 M NaCl (≥99% from Sigma-Aldrich) and 0.1 M NaHCO₃ (≥99.7% from Sigma-Aldrich) in deionized water. In most experiments, we used a concentration of 10 mg mL⁻¹, whereas in clinical trials using intratracheal instillation, the original concentration was used. The lung surfactant with size-reduced particles was prepared by passing the raw surfactant through a 200 nm pore size membrane (Millex PTFE) using a syringe. Dipalmitoylphosphatidylcholine (DPPC) in chloroform, with a stock concentration of 25 mg mL⁻¹, was purchased from Avanti Polar Lipids. The DPPC solution was diluted using chloroform (from Sigma-Aldrich) before deposition at the air–liquid interface in the Langmuir trough. DPPC vesicle suspension in aqueous formulation was prepared using the thin-film method;^[67] see details in Supporting Information. *Trans*-4-[4-(dimethylamino)-styryl]-1-methylpyridinium iodide (DASPI) and dimethyl sulfoxide (DMSO, ≥99.9%) were purchased from Sigma-Aldrich to prepare fluorescently labeled lung surfactant. All surfactant solutions were sealed in glass vials (15 mL, Supelco from Sigma-Aldrich) with PTFE caps and stored in a refrigerator at 2–8 °C. The solutions were used within 3 days of preparation.

Nebulization: VM (Pari eFlow rapid, Germany) and SN (Medspray, Netherlands) nebulization methods were used to produce liquid aerosols, as shown in Figure 1a,b. VM employs a piezoelectric actuator to vibrate an alloy mesh with numerous micrometer-sized holes (average diameter 3.7 ± 0.2 μm, see Figure 1a). The high-frequency vibration of the mesh forced the solution from the reservoir through the holes,^[68] generating aerosols with a median droplet size of 7.0 ± 0.3 μm (Figure S8, Supporting Information). Differently, SN method produces aerosols by mechanically pushing the solution through micrometer-sized holes (average diameter of 2.0 ± 0.1 μm) fabricated on a silicon wafer using semiconductor technology^[27,65] (Figure 1b). The median size of aerosols generated by SN was 13.1 ± 0.8 μm (Figure S8, Supporting Information). Note that droplet coalescence may occur during the production of the drug aerosols in both nebulization methods (Video S4, Supporting Information).

Size Distribution Measurement: To measure the particle size distribution of lung surfactant from different nebulization methods, aerosols were first

collected in a 15 mL centrifuge tube. The collected aerosol solution was then dripped into the Mastersizer 2000SM (Malvern) flow cell. The particle size distribution of surfactant was determined by light scattering.

Langmuir–Wilhelmy Balance: A modified Langmuir–Wilhelmy balance setup was employed to investigate the dynamic activities of the lung surfactant. The trough, constructed from Teflon, measured 210 mm in length, 45 mm in width, and 50 mm in depth. The Teflon barrier had a thickness of 10 mm and a width of 45 mm (same width as the trough). To prevent leakage of the lipid films at the interface, a thin layer of hydrophobic rubber (ELITE Zhermack) was coated to the Teflon barrier (Figure S2, Supporting Information). The barrier was driven by a stepper motor, and the speed of movement can be adjusted within the range of 0.1–20 mm s⁻¹ (corresponding to 2.7–540 cm² min⁻¹ in surface area change). A constant temperature of 37 °C of liquid in the trough was achieved using a chiller (A40 Thermo Scientific). A transparent Plexiglas cover was placed over the trough to reduce the liquid evaporation. Surface tension was measured using a platinum Wilhelmy plate with dimensions of 20 × 10 × 0.18 mm, equipped on a tensiometer (KRUSS, GmbH), see details in Supporting Information.

Lung Surfactant Deposition in the Trough: Instead of directly depositing surfactant aerosols onto the air–liquid interface in the Langmuir trough, a collected aerosol solution was applied to the interface using a Teflon microtube (inner diameter 1.06 mm) connected to a glass syringe (1 mL, SGE gastight) driven by a syringe pump (Harvard PHD 2000), as shown in Figure 1c. This method allows for precise control of the amount of the deposited surfactant.

Confocal Laser Scanning Microscope: The lung surfactant was labeled with DASPI for confocal microscopy imaging.^[69,70] Briefly, DASPI was dissolved in a 1:1 v/v mixture of water and DMSO to obtain a concentration of 1 mM. The lung surfactant solution was then mixed with the DASPI solution, resulting in a final DASPI concentration of 0.005 mM. The labeled solution was then incubated at 2–8 °C for 2 days before measurements were conducted. Fluorescent images were captured using a confocal microscope (Leica TCS SP8) with an excitation wavelength of 448 nm and an emission filter with a wavelength range of 520–625 nm. All images were processed using ImageJ software.

Film Thickness Measurement: To measure the surfactant film thickness during compression–expansion cycles, the Langmuir trough was equipped with an ellipsometer (Multiskop). Polarized light with a wavelength of 632.8 nm was reflected off the surfactant-covered interface and detected by a detector. The laser spot was fixed at the center of the trough. The incident angle of the light was varied near the Brewster angle of water (≈53°), ranging from 48° to 56°. Film thickness was calculated from the measured Δ and Ψ values using a custom Python program.

Surface Flow Measurement: The surface flow field was measured using the PIV technique. Hollow glass particles (diameter 100 μm, from LabVision GmbH) coated with silver were initially distributed at the air–liquid interface formed in a Petri dish (52 mm in diameter). The lung surfactant solution was introduced onto the interface using a Teflon-tipped needle positioned above the surface. Particle movement was captured by a fast camera (MIRO M310) at a frame rate of 3000 frames per second. The velocity field was determined using a home-made MATLAB algorithm which combines with analyzing the images using the PIVlab, an open-source software based on MATLAB.^[71]

Statistical Analysis: The surface tension measurements presented in this work were averaged from 2–3 independent experiments. The standard deviations in surface tension were small and within the symbol sizes in the figures. In total, ≈50 experimental tests were conducted to characterize surfactant behavior at the air–liquid interface. The standard deviation in film thickness measurements using ellipsometry was based on 3–5 different measurements.

Supporting Information

Supporting Information is available from the Wiley Online Library or from the author.

Acknowledgements

This work was supported by Dutch Research Council NWO IPP Grant (Innovative Nanotech Sprays, ENPPS.IPP.019.001). K.X. gratefully acknowledges the funding support from Marie Skłodowska-Curie Actions postdoctoral fellowship (no.101150851). K.X. also acknowledges M. Tuijl and K. van Nieuwland from Technologie Centrum at University of Amsterdam for fabricating the Langmuir trough, P. Kolpakov for the assistance of surface tension measurement, and L. Gao for the help of schematic drawing.

Conflict of Interest

The authors declare no conflict of interest.

Author Contributions

Kaili Xie: conceptualization (equal); data curation (equal); formal analysis (equal); investigation (equal); methodology (equal); visualization (equal); writing—original draft (equal); writing—review and editing (equal). **Thijs Varkevisser:** data curation (equal); formal analysis (equal); methodology (equal); visualization (equal); writing—original draft (equal). **Antoine Deblais:** formal analysis (equal); visualization (equal); writing—original draft (supporting); writing—review and editing (equal). **Wes Onland:** investigation (equal); methodology (equal); resources (equal); writing—review and editing (equal). **Anton H. van Kaam:** methodology (equal); resources (equal); writing—review and editing (equal). **Daniel Bonn:** conceptualization (equal); formal analysis (equal); funding acquisition (equal); methodology (equal); project administration (equal); supervision (equal); writing—review and editing (equal). **Cees J. M. van Rijn:** conceptualization (equal); formal analysis (equal); funding acquisition (equal); methodology (equal); project administration (equal); supervision (equal); writing—original draft (equal); writing—review and editing (equal).

Data Availability Statement

The data that support the findings of this study are available in the supplementary material of this article.

Keywords

aerosol deliveries, dynamic surface tensions, lung surfactants, nebulizations, structural integrities

Received: January 10, 2025

Revised: April 10, 2025

Published online: April 29, 2025

- [1] B. Meyrick, L. Reid, *Br. J. Dis. Chest* **1970**, *64*, 121.
- [2] Jon Goerke, L. Surfactant, *Biochim. Biophys. Acta, Rev. Biomembr.* **1974**, *344*, 241.
- [3] N. Sever, G. Miličić, N. O. Bodnar, X. Wu, T. A. Rapoport, *Mol. cell* **2021**, *81*, 49.
- [4] J. A. Zasadzinski, J. Ding, H. E. Warriner, F. Bringezu, A. J. Waring, *Curr. Opin. Colloid Interface Sci.* **2001**, *6*, 506.
- [5] J. Dyer, *Pharm. Ther.* **2019**, *44*, 12.
- [6] F. J. K. Gnzineko, M. S. Valentine, C. K. Tho, S. R. Chindal, S. Boc, S. Dhapare, M. Abdul Motalib Momin, A. Hassan, M. Hindle, D. R. Farkas, P. W. Longest, R. L. Heise, *J. Aerosol Med. Pulm. Drug Delivery* **2020**, *33*, 314.

- [7] J. D. Horbar, L. T. Greenberg, J. S. Buzas, D. E. Y. Ehret, R. F. Soll, E. M. Edwards, *Pediatrics* **2024**, *153*, e2023064153.
- [8] D. G. Sweet, V. P. Carnielli, G. Greisen, M. Hallman, K. Klebermass-Schrehof, E. Ozek, A. Te Pas, R. Plavka, C. C. Roehr, O. D. Saugstad, U. Simeoni, C. P. Speer, M. Vento, G. H. A. Visser, H. L. Halliday, *Neonatology* **2023**, *120*, 3.
- [9] A. M. A. Elhissi, J. Giebultowicz, A. A. Stec, P. Wroczynski, W. Ahmed, M. Albed Alhnan, D. Phoenix, K. M. G. Taylor, *Int. J. pharm.* **2012**, *436*, 519.
- [10] R. Hentschel, K. Bohlin, A. van Kaam, H. Fuchs, O. Danhaive, *Pediatr. Res.* **2020**, *88*, 176.
- [11] G. Enhorning, A. Shennan, F. Possmayer, M. Dunn, C. P. Chen, J. Milligan, *Pediatrics* **1985**, *76*, 145.
- [12] M. X. Zhang, R. A. Bem, T. Huijgen, R. Klein-Blommert, D. Bonn, C. J. M. van Rijn, *Respir. Care* **2024**, *70*, 327.
- [13] S. Minocchieri, S. Knoch, W. Michael Schoel, M. Ochs, M. Nelle, *Pediatr. Pulmonol.* **2014**, *49*, 348.
- [14] M. C. Hütten, E. Kuypers, D. R. Ophelders, M. Nikiforou, R. K. Jellema, H. J. Niemarkt, C. Fuchs, M. Tservistas, R. Razetti, F. Bianco, B. W. Kramer, *Pediatr. Res.* **2015**, *78*, 664.
- [15] F. Bianco, F. Salomone, I. Milesi, X. Murgia, S. Bonelli, E. Pasini, R. Dellacà, M. Luisa Ventura, J. Pillow, *Respir. Res.* **2021**, *22*, 1.
- [16] F. J. Walther, H. Chan, J. R. Smith, M. Tauber, A. J. Waring, *Sci. Rep.* **2021**, *11*, 16439.
- [17] S. Anderson, P. Atkins, P. Bäckman, D. Cipolla, A. Clark, E. Daviskas, B. Disse, P. Entcheva-Dimitrov, R. Fuller, I. Gonda, H. Lundbäck, B. Olsson, J. Weers, *Pharmacol. Rev.* **2022**, *74*, 48.
- [18] F. J. Walther, A. J. Waring, *Front. Pediatr.* **2022**, *10*, 923010.
- [19] C. Kleinstreuer, Z. Zhang, J. F. Donohue, *Annu. Rev. Biomed. Eng.* **2008**, *10*, 195.
- [20] J. B. Fink, K. W. Stapleton, *J. Aerosol Med. Pulm. Drug Delivery* **2024**, *37*, 140.
- [21] S. Kooij, A. Astefanei, G. L. Corthals, D. Bonn, *Sci. Rep.* **2019**, *9*, 6128.
- [22] L. Vecellio, *Breathe* **2006**, *2*, 252.
- [23] J. Jane Pillow, S. Minocchieri, *Neonatology* **2012**, *101*, 337.
- [24] J. J. Cummings, E. Gerday, S. Minton, A. Katheria, G. Albert, J. Flores-Torres, M. Famuyide, A. Lampland, S. Guthrie, D. Kuehn, J.-H. Weitkamp, P. Fort, E. G. A. Jawdeh, R. M. Ryan, G. C. Martin, J. R. Swanson, N. Mulrooney, F. Eyal, D. Gerstmann, P. Kumar, G. E. Wilding, E. A. Egan, AERO-02 STUDY INVESTIGATORS, *Pediatrics* **2020**, *146*, e20193967.
- [25] R. Tenchov, R. Bird, A. E. Curtze, Q. Zhou, *ACS Nano* **2021**, *15*, 16982.
- [26] S. P. Hertel, G. Winter, W. Friess, *Adv. Drug Delivery Rev.* **2015**, *93*, 79.
- [27] D. M. Klein, A. Poortinga, F. M. Verhoeven, D. Bonn, *Chem. Phys.* **2021**, *547*, 111192.
- [28] C. J. M. van Rijn, K. E. Vlaming, R. A. Bem, R. J. Dekker, A. Poortinga, T. Breit, S. van Leeuwen, W. A. Ensink, K. van Wijnbergen, J. L. van Hamme, D. Bonn, T. B. H. Geijtenbeek, *Sci. Rep.* **2023**, *13*, 8851.
- [29] F. J. Walther, A. J. Waring, *Am. J. Physiol.* **2024**, *327*, L883.
- [30] T. Haller, P. Dietl, H. Stockner, M. Frick, N. Mair, I. Tinhofer, A. Ritsch, G. Enhorning, G. Putz, *Am. J. Physiol.* **2004**, *286*, L1009.
- [31] E. Parra, J. Pérez-Gil, *Chem. Phys. Lipids* **2015**, *185*, 153.
- [32] S. Hertel, T. Pohl, W. Friess, G. Winter, *Eur. J. Pharm. Biopharm.* **2014**, *87*, 386.
- [33] R. Respaud, L. Vecellio, P. Diot, N. Heuzé-Vourc'h, *Expert Opin. Drug Delivery* **2015**, *12*, 1027.
- [34] C. Stefaniu, G. Brezesinski, H. Möhwald, *Adv. Colloid Interface Sci.* **2014**, *208*, 197.
- [35] A. G. Bykov, O. Y. Milyaeva, N. A. Isakov, A. V. Michailov, G. Loglio, R. Miller, B. A. Noskov, *Colloids Surf. A* **2021**, *611*, 125851.
- [36] C. Autilio, M. Echaide, A. Cruz, C. Garca-Mouton, A. Hidalgo, E. Da Silva, D. De Luca, J. B. Sørli, J. Pérez-Gil, *Sci. Rep.* **2021**, *11*, 728.

- [37] A. Z. Stetten, G. Moraca, T. E. Corcoran, S. Tristram-Nagle, S. Garoff, T. M. Przybycien, R. D. Tilton, *J. Colloid Interface Sci.* **2016**, 484, 270.
- [38] J. A. Staton, S. R. Dungan, *Langmuir* **2018**, 34, 9961.
- [39] K. Yee, C. Lee, *Annu. Rev. Phys. Chem.* **2008**, 59, 771.
- [40] T. P. Stevens, R. A. Sinkin, *Chest* **2007**, 131, 1577.
- [41] H. Ritacco, D. Langevin, H. Diamant, D. Andelman, *Langmuir* **2011**, 27, 1009.
- [42] A. Zore, P. Geng, M. R. Van De Mark, *Polymers* **2022**, 14, 2302.
- [43] J. Pérez-Gil, *Biochim. Biophys. Acta* **2008**, 1778, 1676.
- [44] C. O. Ciutara, S. V. Iasella, B. Huang, S. Barman, J. A. Zasadzinski, *Proc. Natl. Acad. Sci.* **2023**, 120, e2309900120.
- [45] R. Wüstneck, J. Perez-Gil, N. Wüstneck, A. Cruz, V. B. Fainerman, U. Pison, *Adv. Colloid Interface Sci.* **2005**, 117, 33.
- [46] A. Cruz, L.-A. Worthman, A. G. Serrano, C. Casals, K. M. W. Keough, J. Perez-Gil, *Eur. Biophys. J.* **2000**, 29, 204.
- [47] D. Schürch, O. L. Ospina, A. Cruz, J. Pérez-Gil, *Biophys. J.* **2010**, 99, 3290.
- [48] F. Brochard-Wyart, P.-G. de Gennes, O. Sandre, *Phys. A* **2000**, 278, 32.
- [49] H. Isambert, *Phys. Rev. Lett.* **1998**, 80, 3404.
- [50] M. Roché, Z. Li, I. M. Griffiths, S. Le Roux, I. Cantat, A. Saint-Jalmes, H. A. Stone, *Phys. Rev. Lett.* **2014**, 112, 208302.
- [51] B. Marie Wiebe, H. Laursen, *Microsc. Res. Tech.* **1995**, 32, 255.
- [52] H. Douafer, V. Andrieu, J. Michel Brunel, *J. Controlled Release* **2020**, 325, 276.
- [53] R. A. Pleasants, D. R. Hess, *Respir. Care* **2018**, 63, 708.
- [54] C. M. Njeru, J. M. Ansermino, W. M. Macharia, D. T. Dunsmuir, *BMC Pediatr.* **2022**, 22, 1.
- [55] F. Possmayer, Y. Y. Zuo, R. A. W. Veldhuizen, N. O. Petersen, *Chem. Rev.* **2023**, 123, 13209.
- [56] A. G. Serrano, J. Pérez-Gil, *Chem. Phys. Lipids* **2006**, 141, 105.
- [57] S. Schürch, F. H. Y. Green, H. Bachofen, *Biochim. Biophys. Acta* **1998**, 1408, 180.
- [58] A. Stachowicz-Kuśnierz, B. Korchowiec, E. Rogalska, J. Korchowiec, *Adv. Colloid Interface Sci.* **2022**, 304, 102659.
- [59] S. C. Taylor, L. K. Rosselli-Murai, B. Crobeddu, I. Plante, *Sci. Rep.* **2022**, 12, 17599.
- [60] N. J. Greenfield, *Nat. Protoc.* **2006**, 1, 2876.
- [61] K. H. Chang, S.-H. Moon, S. K. Yoo, B. Joo Park, K. Chang Nam, *Pharmaceutics* **2020**, 12, 721.
- [62] M. Brasher, T. M. Raffay, M. D. Cunningham, E. G. Abu Jawdeh, *Children* **2021**, 8, 493.
- [63] A. Parrenin, S. Kooij, C. J. M. van Rijn, D. Bonn, *Phys. Fluids* **2024**, 36, 102233.
- [64] S. Pham, G. T. Ferguson, E. Kerwin, T. Goodin, A. Wheeler, A. Bauer, *J. Aerosol Med. Pulm. Drug Delivery* **2018**, 31, 162.
- [65] V. Komalla, C. Y. J. Wong, I. Sibum, B. Muellinger, W. Nijdam, V. Chaugule, J. Soria, H. Xin Ong, N. A. Buchmann, D. Traini, *Expert Opin. Drug Delivery* **2023**, 20, 1055.
- [66] S. Kooij, C. van Rijn, N. Ribe, D. Bonn, *Sci. Rep.* **2022**, 12, 19296.
- [67] L. Šturm, N. Poklar Ulrih, *Int. J. Mol. Sci.* **2021**, 22, 6547.
- [68] S. Ashraf, M. McPeck, A. D. Cuccia, G. C. Smaldone, *Respir. Care* **2020**, 65, 1419.
- [69] A. Briole, T. Podgorski, B. Abou, *Soft Matter* **2021**, 17, 4525.
- [70] E. Mirzahosseini, M. Grzelka, F. Guerton, D. Bonn, R. Brown, *Sci. Rep.* **2022**, 12, 22197.
- [71] W. Thielicke, R. Sonntag, *J. Open Res. Software* **2021**, 9, 12.